



# The Anelastic Behaviors of Co–Fe–Ni–P Metallic Nano-glasses: Studies on the Viscous Glass–Glass Interfaces

TIAN LI and GUANGPING ZHENG

Structural relaxations of grain boundary and glass–glass interfaces (GGIs) play an important role in the mechanical behaviors of polycrystalline metals and metallic nano-glasses (NGs), respectively. Although the former has been well investigated by anelastic or mechanical spectrum measurement, such meaningful technique has not been applied to characterize the structural relaxation of GGIs in NGs as far. In this work, the structural relaxations in Co–Fe–Ni–P NGs with various average sizes ( $D_{\text{avg}}$ ) of glassy grains are investigated by anelastic measurements, which have been synthesized by a pulse electrodeposition method. The results provide direct evidences that a new glass phase could be formed at interfaces in NGs, as characterized by an activation energy (0.91 eV) for glass transition of GGIs much different than that (1.99 eV) in the interiors of glassy grains. From the analyses on dynamical scaling for mechanical losses ( $Q^{-1}$ ) in the glass and supercooled-liquid (SC-liquid) states, *i.e.*,  $Q^{-1} \propto (\omega)^{-n}$ , where  $\omega$  is the angular frequency, it is suggested that the atomic structures at GGIs in NGs with  $D_{\text{avg}} < 150$  nm could be dominated by solid-like atomic clusters, whereas those in NGs with  $D_{\text{avg}} > 250$  nm might be liquid-like. The size effects on the glass forming ability of NGs are also quantitatively measured by exponents of the dynamical scaling in the SC-liquid state, suggesting that NGs with  $D_{\text{avg}} < 40$  nm could be good glass formers. The atomic structures at GGIs revealed in this work could facilitate the development of NGs with desirable mechanical properties through GGI engineering.

<https://doi.org/10.1007/s11661-022-06781-4>

© The Minerals, Metals & Materials Society and ASM International 2022

## I. INTRODUCTION

METALLIC nano-glasses (NGs) containing nano-sized amorphous grains separated by disordered boundaries or interfaces, are now considered as a new class of nanomaterials,<sup>[1–4]</sup> and have attracted much attention because of their excellent physical properties.<sup>[5,6]</sup> Due to the existence of glass-glass interfaces (GGIs), the mechanical,<sup>[7–21]</sup> magnetic,<sup>[22–24]</sup> and thermodynamic<sup>[25–29]</sup> properties of NGs are much different with those of their melt-quenched counterparts. More importantly, the issues of size limitation and brittleness may be well resolved by introducing sufficient amounts of GGIs, thereby forming bulk metallic NGs with decent ductility.<sup>[30]</sup> Until now, a variety of techniques are developed to prepare NGs, such as inert gas condensation,<sup>[31,32]</sup>

magnetron sputtering,<sup>[33,34]</sup> severe plastic deformation,<sup>[35,36]</sup> and pulse electrodeposition.<sup>[37]</sup> However, it has been proved that the strength of those NGs can be dramatically lower than those of melt-quenched metallic glasses (MGs). For instance, through nanomechanical tests on NGs, Franke *et al.*<sup>[38]</sup> found that there was an increase of plasticity as well as a reduction in hardness. It was also found that NGs were much softer than MGs under indentation, and the formation of primary shear bands was restricted.<sup>[39]</sup> Moreover, Wang *et al.*<sup>[40]</sup> demonstrated that NGs exhibited a plastic strain up to 15 pct under uniaxial tension, whereas their yield strength would also drop from 1.8 to 1.3 GPa. In other words, there is a trade-off between ductility and strength in NGs,<sup>[41–43]</sup> which can pose a great challenge to their structural applications. As far, in comparison to homogenous MGs, the current knowledge on the disordered structures of NGs containing nano-structures is still incomplete, especially at their GGI regions. Therefore, this trade-off dilemma cannot be effectively resolved unless the atomic structures at GGIs are well understood.

It is not until recently that some efforts<sup>[44]</sup> were devoted to studying the interfacial atomic structures in NGs.<sup>[45,46]</sup> For example, Fang *et al.*<sup>[47]</sup> proved the

TIAN LI and GUANGPING ZHENG are with the Department of Mechanical Engineering, The Hong Kong Polytechnic University, Hung Hom, Kowloon, Hong Kong SAR, 10000, P.R. China. Contact e-mail: mmzheng@polyu.edu.hk

Manuscript submitted March 23, 2022; accepted July 23, 2022.

Article published online August 14, 2022

**Table I. Thermodynamic Properties ( $T_g$ ,  $T'_g$ ,  $T_x$  and  $\Delta T = T_x - T_g$ ) of Co–Fe–Ni–P NGs with  $D_{\text{avg}}$  and GGI Volume Fraction  $x$ , and  $\text{Zr}_{57}\text{Cu}_{15.4}\text{Ni}_{12.6}\text{Al}_{10}\text{Nb}_5$  BMG, as Determined by DSC and DMA**

| Properties            | Sample #1 | Sample #2 | Sample #3 | Sample #4        | BMG |
|-----------------------|-----------|-----------|-----------|------------------|-----|
| $D_{\text{avg}}$      | 80 nm     | 140 nm    | 280 nm    | 40 $\mu\text{m}$ | —   |
| $x$                   | 0.76      | 0.58      | 0.29      | 0.01             | —   |
| $T_g$ (K) by DSC      | 530       | 536       | 540       | 550              | 570 |
| $T'_g$ (K) by DMA     | 520       | 526       | 531       | 540              | 560 |
| $T_x$ (K) by DSC      | 626       | 630       | 634       | 637              | 617 |
| $T_x$ (K) by DMA      | 618       | 615       | 621       | 611              | 603 |
| $\Delta T$ (K) by DSC | 96        | 94        | 94        | 87               | 47  |

existence of GGIs from a combined study of positron annihilation spectroscopy and small angle X-ray scattering. They also found a higher content of free volumes at GGIs. This fact was further supported by the molecular dynamics simulations,<sup>[48,49]</sup> which revealed an increase of free volumes at the GGIs. Furthermore, Mossbauer analyses<sup>[50]</sup> confirmed that the interfacial atomic structures could differ from those of melt-quenched counterparts. Nevertheless, characterization of GGIs in NGs is still qualitatively and always requires a reference such as MGs, and particularly, quantitative analysis on the atomic structures at GGIs is currently unavailable.

Anelastic analyses on disordered solids have played an important role in understanding the atomic structures, structural relaxation and glass transition behaviors of MGs.<sup>[51,52]</sup> By measuring their anelastic behaviors through mechanical spectroscopy, the structural properties or defects related to the  $\beta$  relaxation<sup>[53]</sup> and  $\alpha$  relaxation (or the glass transition)<sup>[54]</sup> in MGs can be accurately determined. For example, the activation energies ( $E_a$ ) can be obtained by applying Arrhenius or Vogel–Fulcher–Tammann (VFT) relation to analyze the internal friction ( $Q^{-1}$ ) peaks<sup>[54–56]</sup>; the density, sizes, and relaxation time of free-volume defects can be quantitatively measured by dedicated anelastic studies. Although for some MGs, those peaks would not appear in the anelastic measurements, especially for  $\alpha$  relaxations close to the glass transition temperatures ( $T_g$ ),<sup>[57]</sup> alternative methods have been proposed to quantify structural relaxations in MGs through analyses on the mechanical spectrum and dynamical viscosity ( $\eta$ ).<sup>[58–60]</sup> Nonetheless, to the best of our knowledge, such meaningful technique in quantitatively characterizing the structural relaxation of disordered structures has not been utilized to study the atomic structures of GGIs.

In this work, anelastic behaviors related with the structural relaxation of interfaces in Co–Fe–Ni–P metallic NGs are systematically investigated by mechanical spectrum, which have been successfully synthesized by a pulse electrodeposition method. It is found that the atomic structures at GGIs in the NGs are much different with those in the interiors of nano-sized glassy grains, confirming the previous results on NGs that interfacial regions possess excess free volumes. More importantly, this work gives the direct evidence that a new glass phase has formed in NGs since  $E_a$  of  $\alpha$  relaxation or glass

transition at GGIs can be differentiated quantitatively. The size effects on the glass transition and glass forming ability (GFA) of NGs are also studied by the measurements on  $\eta$  and the mechanical spectrum.

## II. EXPERIMENTAL METHODOLOGIES

Co–Fe–Ni–P metallic NGs with a thickness as large as 0.2 mm were fabricated through a pulse electrodeposition method in a conventional three-electrode electrochemical cell. Micro- and nano-structured samples were deposited on the titanium working electrode. A graphite rod was used as the counter electrode and the electrodeposition potential was controlled by saturated calomel electrode. The electrolytic solution was prepared with analytical grade chemical reagents and maintained at 333 K throughout the electroplating processes. The composition of the electrolyte was summarized as follows:  $\text{FeSO}_4 \cdot 7\text{H}_2\text{O}$  0.03 mol/L,  $\text{CoSO}_4 \cdot 7\text{H}_2\text{O}$  0.03 mol/L,  $\text{NiSO}_4 \cdot 6\text{H}_2\text{O}$  0.03 mol/L,  $\text{C}_6\text{H}_5\text{Na}_3\text{O}_7 \cdot 2\text{H}_2\text{O}$  0.2 mol/L,  $\text{H}_3\text{BO}_3$  0.5 mol/L, and  $\text{NaH}_2\text{PO}_4 \cdot \text{H}_2\text{O}$  0.2 mol/L. Solution PH was adjusted down to 4 by adding  $\text{H}_2\text{SO}_4$ . For micro-structured samples, direct current (DC) electrodeposition was applied with a working potential of 0.9 V, and the electroplating process could take up to 24 hours. On the contrary, nano-structured samples were prepared by pulse electrodeposition. A generator was utilized to output pulse signals with a duty cycle of 15 pct at 100 kHz to a potentiostat. The pulse potentials of 3.8, 2.6, and 1.9 V were chosen to fabricate different nano-structured samples. During the pulse electrodeposition, samples with a smaller size of glassy grains could be synthesized when a higher pulse potential was utilized, with the duty cycle and pulse frequency maintained unchanged. A self-designed Teflon mold was used to prepare the sample in rectangular shape (30 mm  $\times$  3.5 mm  $\times$  0.1 mm). All as-prepared micro- and nano-structured samples were mechanically exfoliated. Heat treatments in vacuum were applied on those free-standing specimens at 473 K to relieve internal stresses before anelastic measurements.

The solid states of micro- and nano-structured samples were characterized by X-ray diffraction (XRD, Smartlab, Rigaku, JPN) operated at 45 kV and 250 mA with Cu  $K_\alpha$  radiation ( $\lambda = 0.154$  nm). Scanning electron

microscopy (SEM, Vega 3, Tescan, BRQ) equipped with energy dispersive spectroscopy (EDS) was used to observe the micro- or nano-structures in the cross sections of specimens and determine the overall chemical compositions. High-resolution images on glassy grains less than 100 nm in diameters were taken by transmission electron microscopy (TEM, Jem-2011, Joel, JPN). Needle-shaped samples for atom probe tomography (APT, Cameca, Leap 5000 HR, FRA) were fabricated by lift-outs and annular milled in a focused ion beam (FIB-SEM, Scios, FEI, OR). The APT characterization was performed in a local electrode atom probe. The specimens were analyzed at 70 K in a voltage mode, at a repetition rate of 200 kHz, a fraction of 20 pct, and an evaporation detection rate of 0.3 pct atom per pulse. The data analysis workstations AP Suite 6.1 was used for creating the 3D reconstructions and data analysis. The thermodynamic properties of samples were measured by differential scanning calorimetry (DSC, Q200, TA Instruments, MN) at a heating rate of 10 K/min. The anelastic behavior was evaluated by performing dynamic mechanical analysis (DMA, Q800, TA Instruments, MN). Free-standing samples were mounted on a dual cantilever clamp. A constant oscillating amplitude of 20  $\mu\text{m}$ , at frequencies of 0.2 to 0.8 Hz, was applied on the specimen at 303 K to 673 K under a heating rate of 1 K/min. A 5-min delay time was set at 303 K before each anelastic measurement.

### III. RESULTS AND DISCUSSIONS

#### A. The Structural, Thermodynamic, and Anelastic Properties of NGs

XRD patterns of micro- and nano-structured samples are shown in Figure 1(a). The average sizes ( $D_{\text{avg}}$ ) of glassy grains are determined from their SEM images by calculating the mean diameter of at least 20 micro- or nano-sized grains for each specimen. Glassy grains as identified in the SEM images are randomly chosen to measure their diameters. On the basis of Figures 1(b)

through (e) for samples #1, #2, #3, and #4,  $D_{\text{avg}} = 80 \pm 6$ ,  $140 \pm 13$ ,  $280 \pm 22$  nm, and  $40 \pm 10$   $\mu\text{m}$  are estimated, respectively. A typical broad peak can be observed at  $2\theta \sim 44$  deg in the XRD patterns, which clearly indicates that all samples are fully amorphous. Based on the EDS analysis, chemical compositions of both micro- and nano-structured samples may be written as  $\text{Co}_{58}\text{Fe}_5\text{Ni}_{14}\text{P}_{23}$ , and all elements are found to be uniformly distributed. Low- and high-resolution TEM images for sample #1 are presented in Figures 2(a) through (c), suggesting that glassy grains with sizes less than 50 nm are formed. The selected area electron diffraction (SAED) patterns with a halo ring from Figure 2(d) confirm the amorphous state of heterogeneous structures.

Figures 3(a) through (f) shows the spatial elemental reconstruction at the tip of needle-shaped sample #1. In general, all elements are well distributed throughout the examined region with no dramatic reduction in the total number densities of Co, Ni, Fe, and P elements, suggesting that GGIs do not contain any nanovoids. Furthermore, the elemental concentrations at the position marked as  $\sim 80$  nm, are found to be abnormal, as illustrated by the dash lines in profiles from Figure 3(g), which may be attributed to the existence of GGIs close to that position. An enrichment of Co and Fe atoms goes along with a depletion of Ni and P atoms is characterized in the highlighted region. To be specific, the composition in this abnormal area is estimated to be  $\text{Co}_{56}\text{Fe}_3\text{Ni}_{16}\text{P}_{25}$ , while those in other regions possibly being the grain interiors are averaged to be  $\text{Co}_{54}\text{Fe}_2\text{Ni}_{18}\text{P}_{26}$ . The APT results suggest that the nano-structures in the NGs could be dense and GGIs are expected to possess a chemical composition different than those in the interiors of glassy gains.

The thermodynamic properties of samples #1 to #4 are measured by DSC, as shown in Figures 4(a) and (b).  $T_g$  and  $T_x$  are defined as the onset temperatures of endothermic and exothermic peaks upon cooling and heating, as marked by arrows indicating the abrupt decreases and increases in the tangent of heat-flow

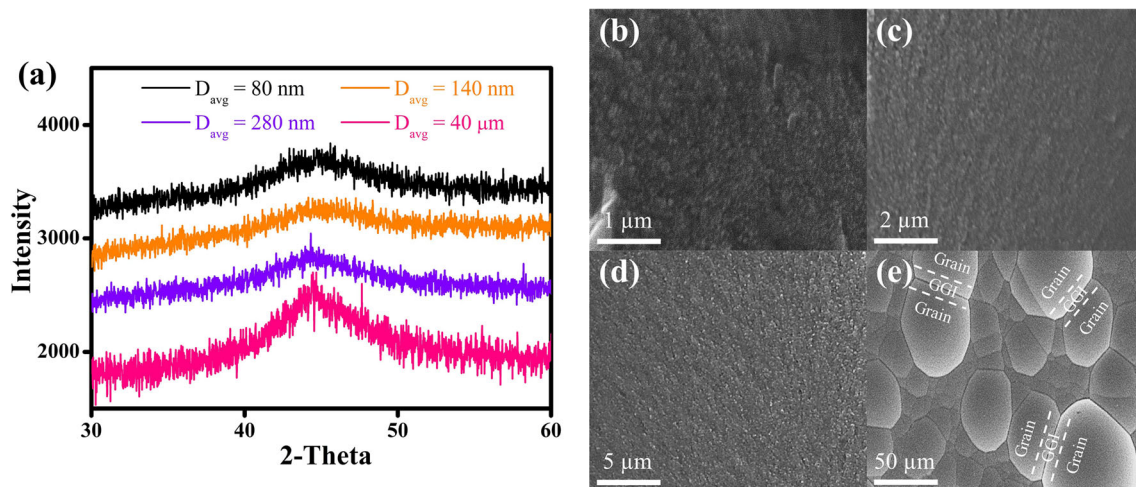


Fig. 1—XRD patterns (a) and SEM images (b) through (e) for samples #1 to #4 with different  $D_{\text{avg}}$  listed in Table I. The labels in (e) illustrate the grain interiors and GGI regions.



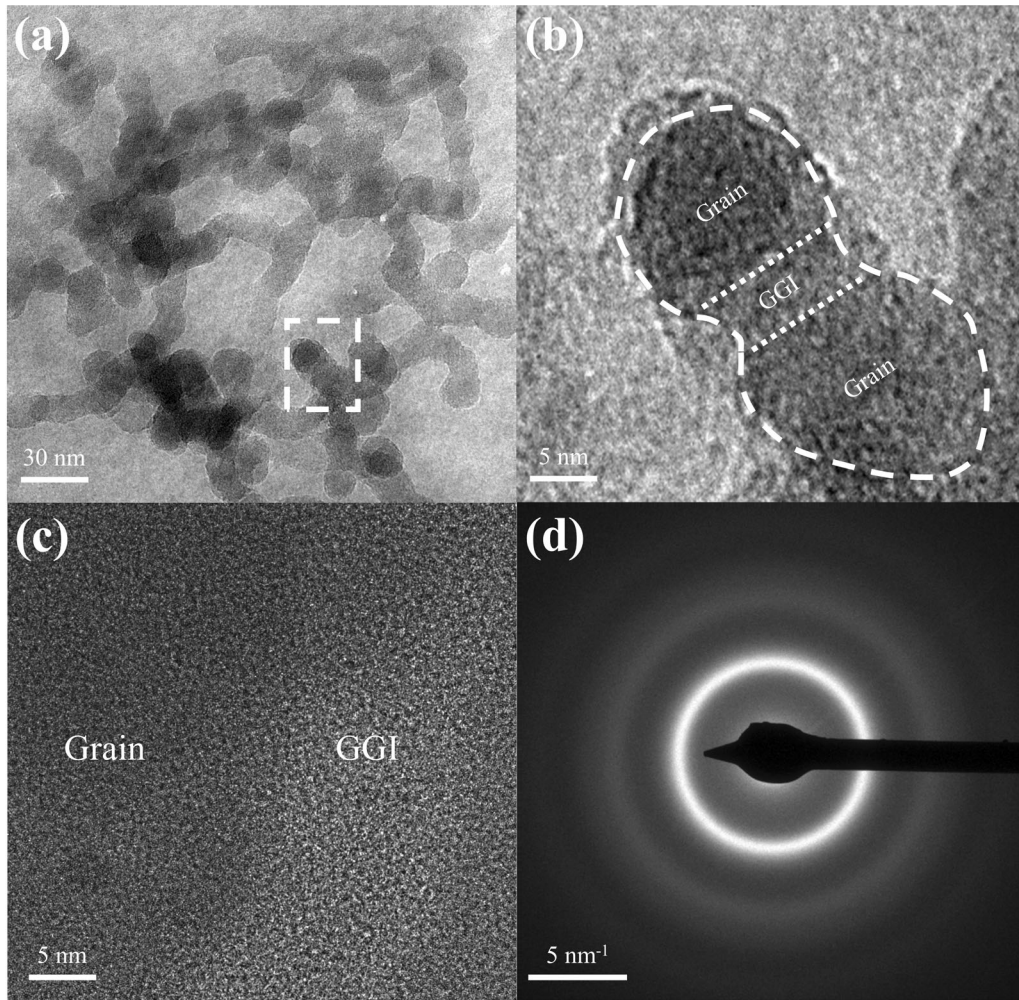


Fig. 2—(a) Low-, and (b) and (c) high-resolution TEM images with (d) SAED analyses on sample #1. The grain interiors and GGI regions marked with a dashed square in (a) are illustrated in (b) with labels.

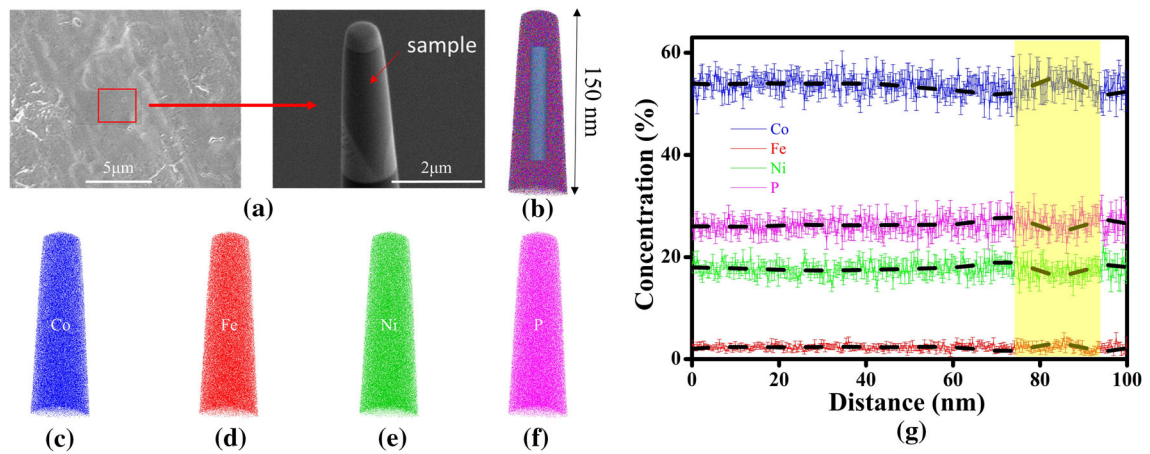


Fig. 3—APT measurements on the chemical compositions of (a) needle-shaped sample #1 with (b) reconstruction of (c) Co, (d) Fe, (e) Ni, and (f) P atoms. (g) Elemental concentration profiles are examined in the cylindrical region shown in (b) with a length of 100 nm; the dash lines (spline-fitting smoothing of data) show the abnormal changes in composition, which suggest the existence of a GGI at the highlighted area or positions.

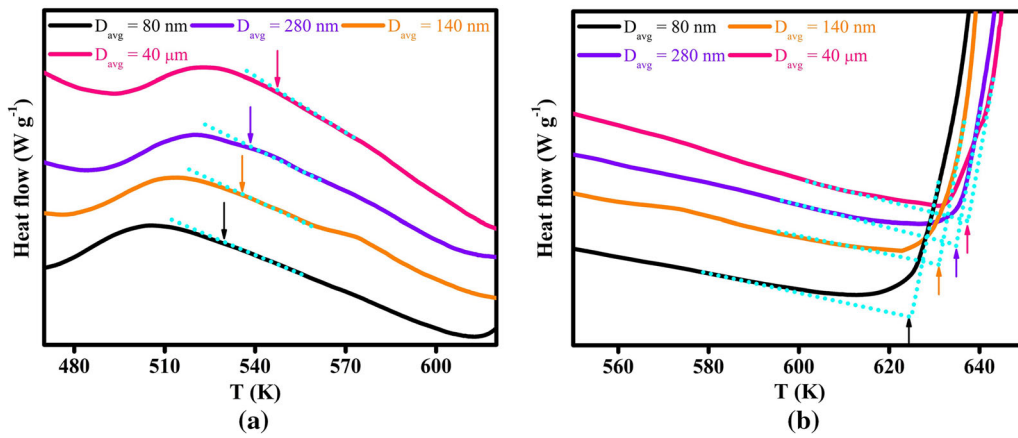


Fig. 4—DSC heat flows for samples #1 to #4 at a heating rate of 10 K/min. (a)  $T_g$  and (b)  $T_x$  are marked by arrows. The dash lines are tangent lines for the heat-flow curves.

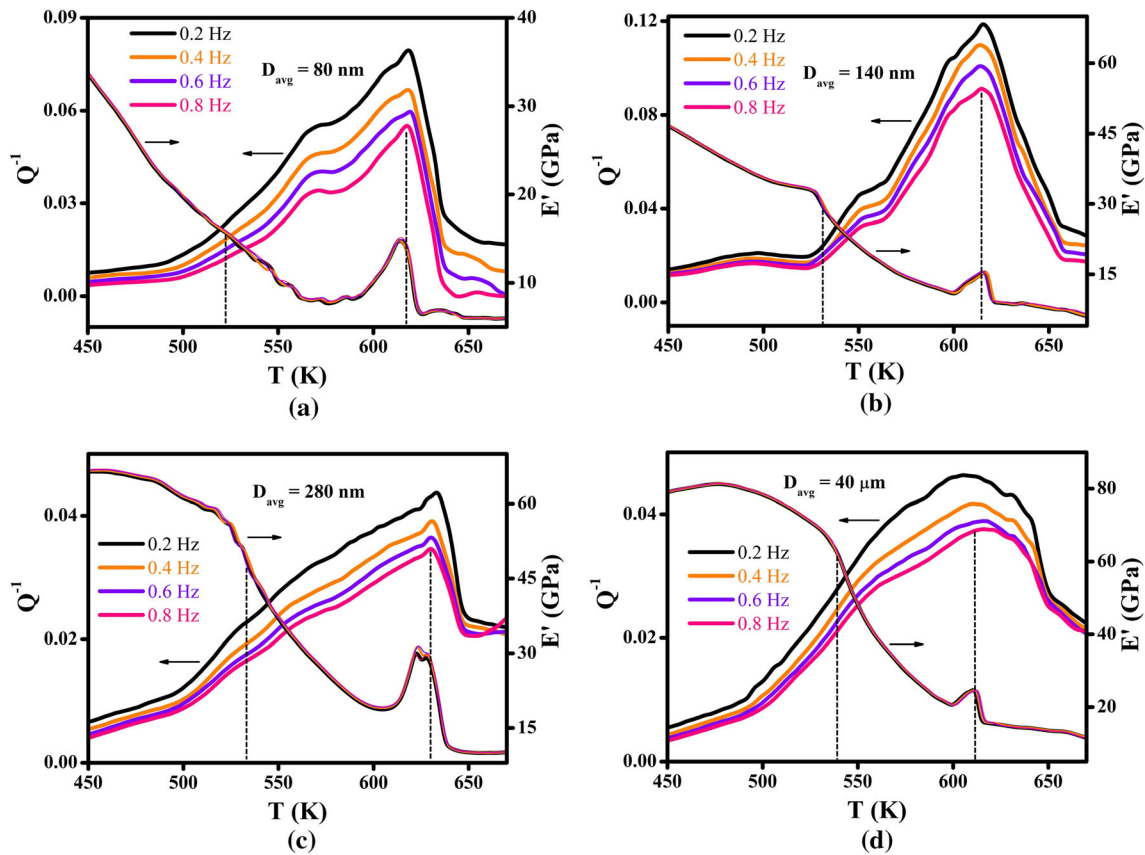


Fig. 5—Internal friction  $Q^{-1}$  and storage modulus  $E'$  at 1 K/min heating rate for (a) through (d) samples #1 to #4, respectively. The dash lines mark the onset of glass transition (left) and crystallization (right).

curves, respectively. The results of thermodynamic properties are listed in Table I. It can be found that both crystallization temperatures ( $T_x$ ) and  $T_g$  decrease with increasing GGI volume fractions  $x$ , which is estimated by assuming that glassy grains are spherical. Based on the thicknesses of GGI regions in micro- and nano-structured samples as estimated from SEM images and APT measurements, respectively, the volume fractions of GGIs and glassy grain interiors are determined.

DMA results for samples #1 to #4 are shown in Figures 5(a) through (d), respectively. The structural transitions and evolutions of atomic structures in Co-Fe-Ni-P samples are well reflected in their anelastic behaviors. A predominant frequency-dependent internal friction ( $Q^{-1}$ ) peak can be found above 600 K, which characterizes the crystallization transformation. It should be noted that the peak position may not be consistent with the crystallization temperature ( $T_x$ )

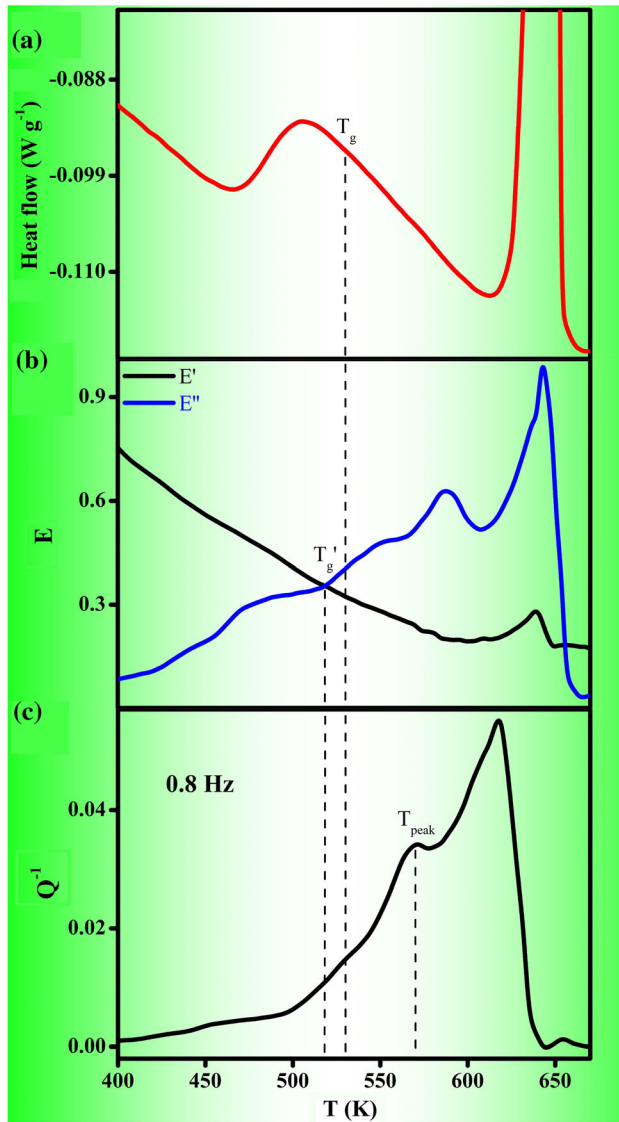


Fig. 6—The glass transition temperatures  $T_g$  and  $T'_g$  for sample #1, as marked with dash lines, are measured by (a) DSC at a heating rate of 10 K/min, and by (b) complex modulus ( $E'$  and  $E''$ ) at a heating rate of 1 K/min, respectively, which are used as references to characterize the (c) temperature-dependent internal friction ( $Q^{-1}$ ) peaks.

determined by DSC and is generally at lower temperature, mainly caused by a lower heating rate. In comparison to samples #3 to #4, the intensities of crystallization peaks for samples #1 to #2 with reduced  $D_{avg}$  are prominent, suggesting that their GGIs could be structured differently that lead to an increase in  $Q^{-1}$  close to  $T_x$ . Below  $T_x$ , a sub-peak can be observed at  $T_{peak}$  close to  $T_g$  for samples #1 to #2, which slightly shifts to higher temperature with increasing frequency, and it should result from the glass transition. With increasing  $D_{avg}$ , such relaxation peak cannot be distinguished for samples #3 to #4, indicating that GGIs significantly affect the glass transitions in NGs. Moreover, an increase in the intensity of relaxation peak with increasing GGI volume fractions  $x$  also reveals that the structural relaxations at GGIs differ from those inside

glassy grains. As a result, the changes of storage modulus ( $E'$ ) for samples #1 to #4 are significantly different. At temperature above 500 K, a dramatic reduction of  $E'$  from 60 to 12 GPa for samples #3 to #4 has been determined. Similarly, an abrupt modulus change is observed for sample #2 as it transforms from the glass state into supercooled-liquid (SC-liquid) state at  $T_g$ . In contrast, sample #1 is gradually softened from 20 to 10 GPa, suggesting that GGIs are less dense with a much lower stiffness. Therefore, based on anelastic measurements, it may be concluded that interfaces in NGs have different atomic structures as compared to those at the interiors of glassy grains, and GGIs could play an important role during structural relaxation.

Figures 6(a) through (c) shows the comparison on the glass transition temperatures determined by DSC and DMA. Taking sample #1 as an example,  $T_g$  is identified at the edge of endothermic shoulder of heat-flow curves, which is about 530 K. Apart from this determination, the glass transition temperature can be also defined as the turnover between the solid-like and liquid-like atomic structures, judging the fact that a solid is condensed matter whose resistance to shear stress is finite whereas that of a liquid is close to zero. The transition point of this distinction is referred as the temperature  $T'_g$  that the storage modulus  $E' = E \cdot \cos\delta$  and loss modulus  $E'' = E \cdot \sin\delta$ <sup>[61]</sup> normalized by their respective maximum are crossing over. Following this principle at a lower heating rate (1 K/min),  $T'_g$  measured to be  $\sim 520$  K is slightly lower than  $T_g$  determined from DSC (with a higher heating rate of 10 K/min). In general, the onset temperatures for glass transition as well as crystallization transformation increase with increasing heating rate, suggesting that  $T'_g$  should be consistent with  $T_g$ . Moreover, it is found that the  $Q^{-1}$  peak at  $\sim 560$  K, associated with glass transition, locates at  $T_{peak}$  above  $T_g$ . In MG, it is suggested that the phase transition from the glass to the liquid states is a de-frozen process, and the amount of viscous liquids will increase at elevated temperatures above  $T_g$ ; Only at an intermediate temperature with a critical amount of liquids, the internal friction will reach a maximum, thereby resulting in an apparent  $Q^{-1}$  peak at  $T_{peak}$  above  $T_g$ , i.e.,  $T_g < T_{peak} < T_x$ .

### B. The Influences of Sizes of Glassy Grains on the Structural Relaxation of GGIs

In order to have an in-depth understanding on the atomic structures of GGIs, anelastic behaviors of electrodeposited samples are further investigated. Previous work<sup>[47,50,62]</sup> has suggested that GGIs in NGs are similar with glassy grains that their atomic structures are disordered and could be in different amorphous phases, which may be considered as atomic clusters containing free-volume defects. Under an applied oscillating stress  $\sigma(t) = \sigma_o \sin(\omega t + \varphi)$ , where  $\sigma_o$  is the stress amplitude,  $\omega = 2\pi f$  is the angular frequency and  $\varphi$  is the phase lag, the local responses (at position  $x$ ) of clusters at GGIs and in the interiors of glassy grains can be described by the equation of motion, as follows:



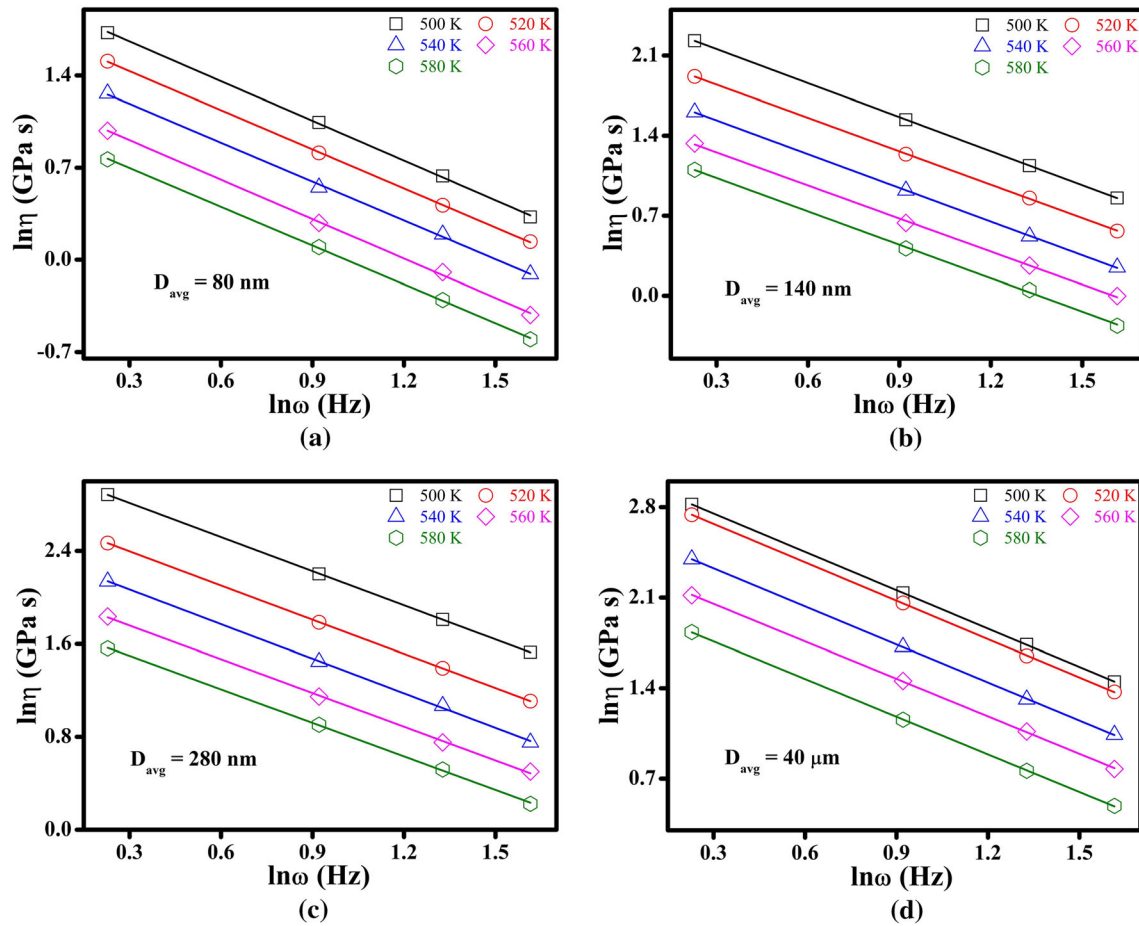


Fig. 7—Log-log plots of dynamical viscosity  $\eta$  vs angular frequency  $\omega$  for (a) through (d) samples #1 to #4, respectively, at temperatures close to  $T_g$ .

$$\rho \ddot{x} + \gamma \cdot \dot{x} + kx = F(t), \quad [1]$$

where  $\rho$  is the density of clusters,  $k$  is the dynamic restoring coefficient of the clusters whose resonant frequency is  $\omega_0 = (k/\rho)^{1/2}$  and  $\gamma = \eta/A$ , where  $\eta = G/\omega^{[63]}$  and  $A$  is the cross sections of the clusters.  $F(t)$  is the harmonic force per volume exerted on the cluster, and it can be written as follows:

$$F(t) = \alpha_1(\omega, \eta) \alpha_2(\omega, \eta) \cdot \sigma_0 \sin(\omega t + \varphi), \quad [2]$$

where  $\alpha_1(\omega, \eta)$  and  $\alpha_2(\omega, \eta)$  are coupling coefficients (within 0 and 1) related with the viscoelastic properties of those clusters in glassy grains and at GGIs, respectively. In addition, the energy dissipated in a relaxation process is defined as follows:

$$\Delta W = N_0 \int_0^{2\pi/\omega} [\alpha_1(\omega, \eta) \alpha_2(\omega, \eta) \sigma_0 \sin(\omega t + \varphi)] \dot{x} dt, \quad [3]$$

where  $N_0$  is the volume density of clusters at GGIs and in the interiors of glassy grains, and  $Q^{-1} = \Delta W / (\pi \sigma_0^2 / G)$ , where  $G$  is the shear modulus of samples.<sup>[64]</sup> It has been found that  $\eta$  close to  $T_g$  can be scaled with respect to  $\omega$  in the low-frequency range, which is illustrated in Figures 7(a) through (d) for

samples #1 to #4, respectively. Therefore, the dynamical scaling relation for  $Q^{-1}$  can be developed as follows:

$$Q^{-1} \propto (\omega)^{-n}, \quad [4]$$

where index  $n$  is a power-law exponent with  $0 \leq n \leq 1$ , and capable of quantitatively characterizing the structural relaxation in disordered solids. Generally speaking, a higher value of  $n$  is envisaged when the response of clusters to the external mechanical perturbation is more significant. In other words, a lower index  $n$  may stand for those solid-like clusters with large shear modulus while a large index  $n$  may represent those liquid-like clusters with small shear modulus. In comparison to solid-like clusters, liquid-like clusters in glassy materials may refer to atomic clusters containing larger amounts of free volumes induced by more numbers of local quasi-defects in atomic structures.

To better identify the structural relaxations of electrodeposited specimens, index  $n$  are determined from  $Q^{-1}(T)$  with the backgrounds ( $Q_o^{-1}$ ) subtracted, as illustrated in Figures 8(a) through (d). Based on obtained index  $n$  for samples #1 to #4 presented in Figure 8(e), atomic structures at GGIs can be

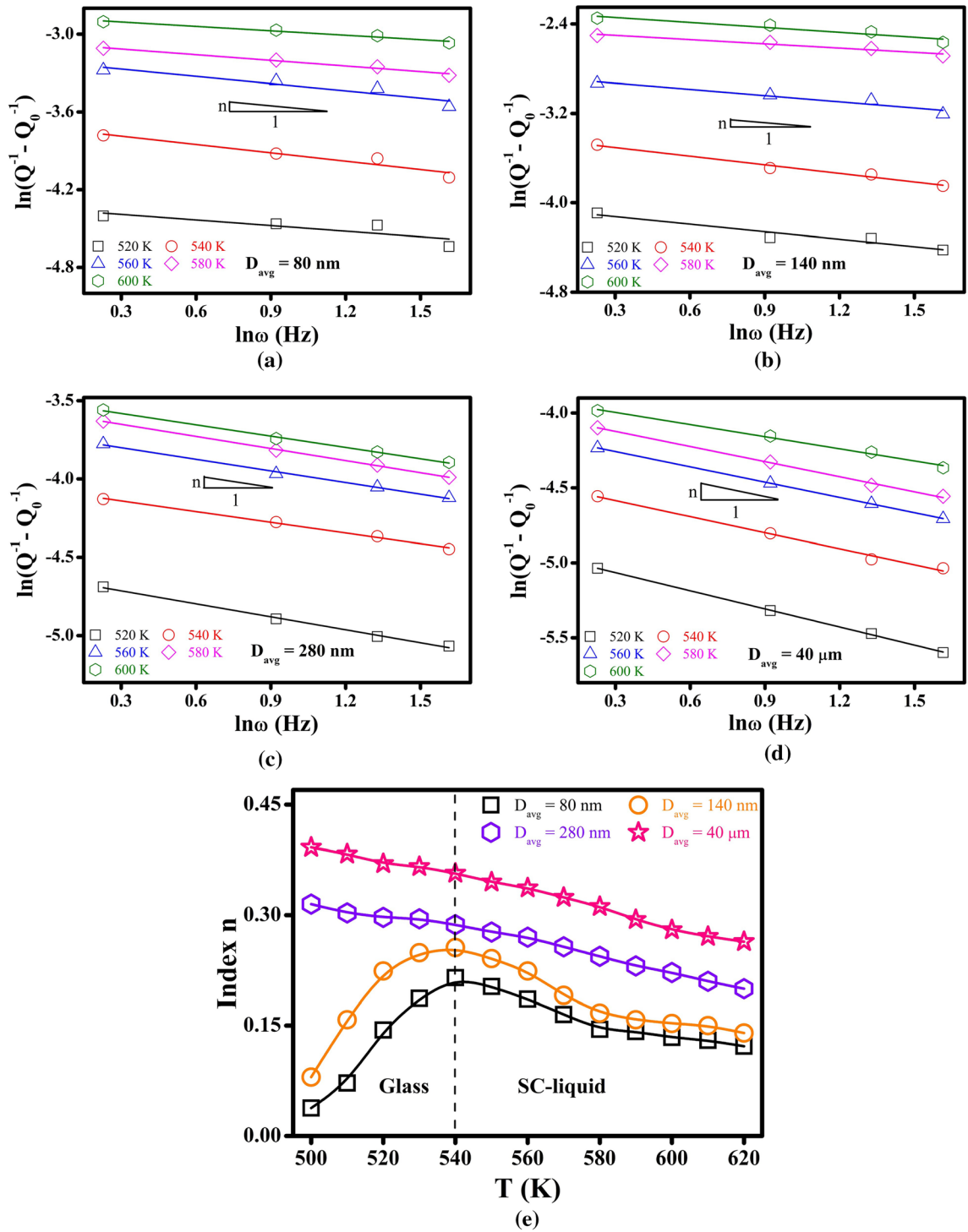


Fig. 8—The dynamical scaling for internal friction  $Q^{-1}$  to  $Q_0^{-1}$  with respect to the angular frequency  $\omega$  for (a) to (d) samples #1 to #4, respectively, at temperatures close to  $T_g$ . (e) Index  $n$  for samples #1 to #4 at temperatures around  $T_g$ ; the dash line marks  $T_g$  and the transition between a glass state and an SC-liquid state.

quantitatively characterized by evaluating the activation energy  $E_a$  of structural relaxations near  $T_g$ . Assuming anelastic relaxation is a typical Debye relaxation,<sup>[59,64]</sup> Eq. [4] is expressed as  $Q^{-1} \sim (\omega\tau)^{-n}$  where  $\tau = \tau_0 \cdot \exp(E_a/k_B T)$  is the relaxation time, and is re-written as follows:

$$\ln Q^{-1} = -n \left( \ln\omega + \ln\tau_0 + \frac{E_a}{k_B T} \right), \quad [5]$$

where  $\tau_0$  is the pre-exponent coefficient and  $k_B$  is Boltzmann constant.  $E_a$  can be determined by a linear



fitting of  $\ln Q^{-1}$  with respect to  $1/T$  close to  $T_g$ , as demonstrated in Figure 9(a). Supposing GGIs in all specimens are in a glass state with a constant activation energy of  $E_{GGI}$  and glassy grains are in another glass state with an activation energy of  $E_{grain}$ , a dual-phase model for samples #1 to #4 containing two glass phases at GGIs and glassy grains can be well established for estimating the activation energy  $E_a$  of glass transition as follows:

$$E_a = (1 - x)E_{grain} + xE_{GGI}. \quad [6]$$

As shown in the inset of Figure 9(b),  $E_{grain}$  and  $E_{GGI}$  are determined to be 1.99 eV and 0.91 eV, respectively. The results are consistent with previous experimental<sup>[47]</sup> and simulation<sup>[42]</sup> work that the atomic structures of GGIs could have excess free volumes than those of glassy grains or BMGs, as reflected by  $E_{GGI} < E_{grain}$ . Thus, it is evidential glass transition and structural

relaxation would prefer to initiate at GGIs, instead of the interiors of glassy grains.

It has been seen from Figure 8(e) that the dependence of index  $n$  on temperature is similar for all samples at the SC-liquid state ( $T_g < T < T_x$ ) due to the presence of dominant liquid-like clusters, whereas at the glass state, the structural relaxations of samples #1 to #2 are much different than those in samples #3 to #4. Figure 8(e) clearly shows that the index  $n$  for samples #1 to #2 exhibits a local maximum at  $\sim 540$  K, which cannot be observed for samples #3 to #4. Since the previous analyses on  $E_a$  have suggested glass transition prefers to initiate at GGIs when temperature is close to  $T_g$ , such a huge change on index  $n$  is most likely to be contributed by GGIs. In other words, the atomic structures at interfaces in samples #1 to #2 and samples #3 to #4 are much different. Therefore, it may be concluded that the GGI phases are strongly dependent on  $D_{avg}$  of Co-Fe-Ni-P samples, and the aforementioned

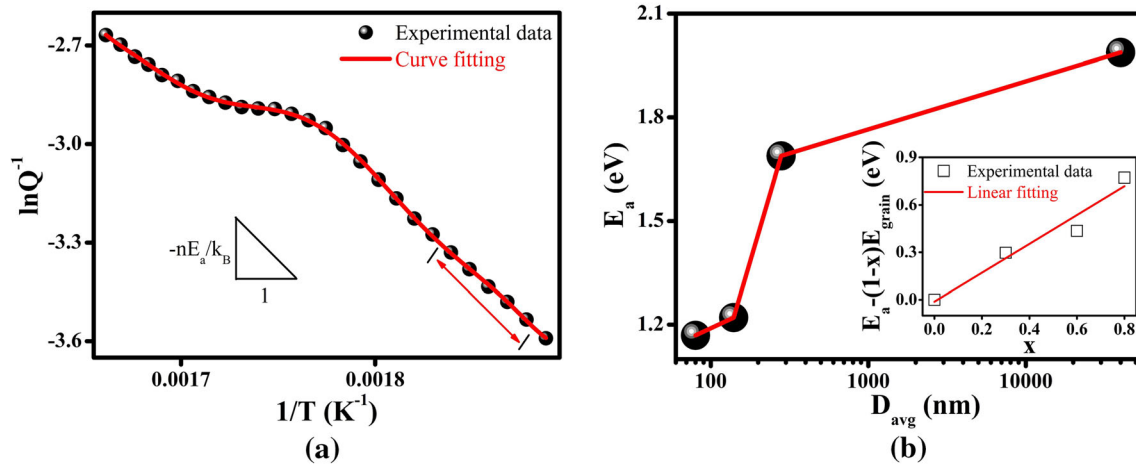


Fig. 9—(a) The relation between  $\ln Q^{-1}$  and temperature near  $T_g$  in sample #1 at  $f = 0.2$  Hz. (b) Activation energies  $E_a$  of glass transition for samples #1 to #4; the inset is the plots for Eq. [6] with  $E_{grain} = 1.99$  eV that determine  $E_{GGI}$ .

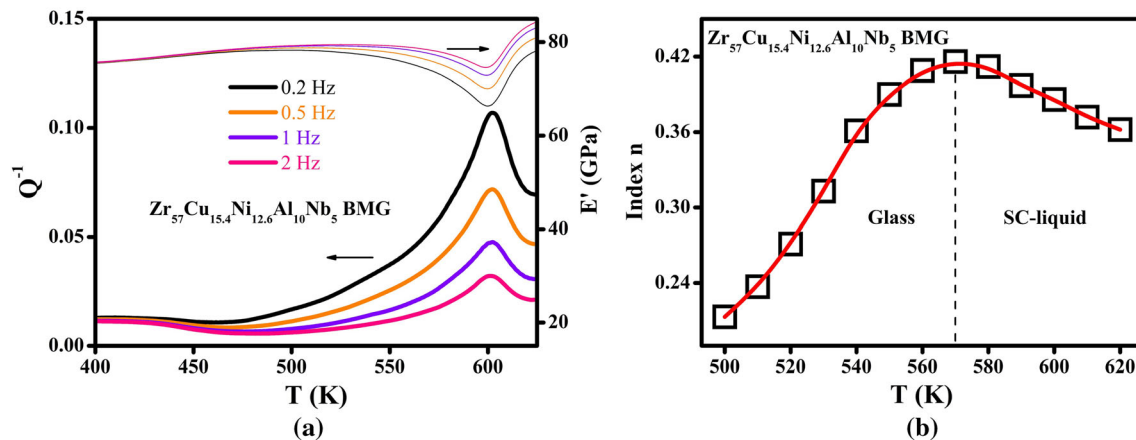


Fig. 10—(a) Mechanical spectra measured with a heating rate of 0.3 K/min, (b) plots of index  $n$  with respect to temperature, for  $Zr_{57}Cu_{15.4}Ni_{12.6}Al_{10}Nb_5$  BMG; the dash line marks  $T_g$  and the transition between a glass state and an SC-liquid state.

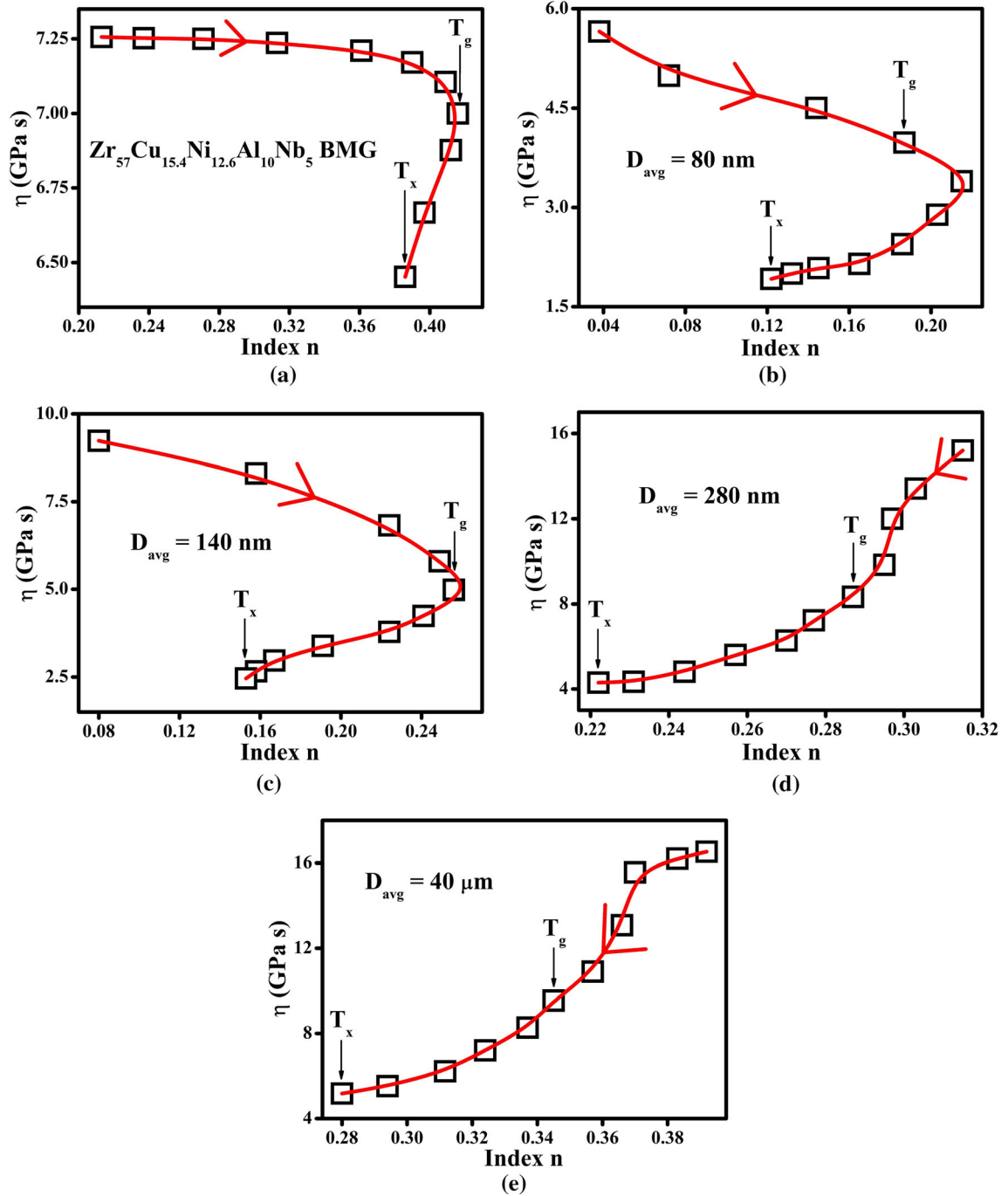


Fig. 11—The plots of index  $n$  with respect to dynamic viscosity  $\eta$  (at 0.2 Hz) for (a)  $Zr_{57}Cu_{15.4}Ni_{12.6}Al_{10}Nb_5$  BMG, (b) through (e) samples #1 to #4 with different  $D_{avg}$ , respectively. The arrow in the fitted curve indicates the increase in temperature along the curve. The arrows pointing to the data points show the temperatures  $T_g$  and  $T_x$  at which the glass transition and crystallization occur, respectively.

dual-phase composite model (Eq. [6]) may be over simplified to describe them in NGs.

To reveal such a difference in the atomic structures of GGIs from micro- and nano-structured samples as determined by the index  $n$  at  $T < T_g$ , origin of this local maximum of index  $n$  is further studied by investigating the anelastic behaviors of a well-established  $Zr_{57}Cu_{15.4}Ni_{12.6}Al_{10}Nb_5$  BMG (commercial products of Liquid-metal Technologies Inc.) without GGIs (or with

homogeneous glassy structure). It is worth noting that its glassy structures dominated by solid-like atomic clusters have been well established and are characterized to be thermodynamically stable. Based on the mechanical spectra of BMG shown in Figure 10(a), its index  $n$  could be determined, which have been illustrated in Figure 10(b). Particularly at  $T_g$  ( $\sim 560$  K, in Table I), the index  $n$  for BMGs is found to be 0.41 and can be identified from the plots presented in Figure 11(a) as well.

It has been previously known<sup>[51]</sup> that  $\alpha$  relaxation is attributed to the activation of quasi-defects in solid-like clusters at  $T < T_g$  and index  $n$  is specifically employed to reflect such structural relaxation during the glass transition. In the glass state at  $T < T_g$ , those quasi-defects in solid-like clusters could be activated by thermal activation at elevated temperature and transform into liquid-like clusters with extra free volumes, resulting in a larger index  $n$  and a lower viscosity with increasing temperature, as demonstrated in Figures 10(b) and 11(a). In the SC-liquid state at  $T_g < T < T_x$ , liquid-like clusters would be dominant in the BMG and the viscosity (or the dynamical relaxation time) of clusters in its atomic structures could be decreased, resulting in a lower index  $n$  with increasing temperature. As a result, the maximum of index  $n$  at 570 K close to  $T_g$  is identified for the BMG. This maximum of index  $n$  at  $T_g$  is closely related to the solid-like clusters in BMG that greatly influence its structural relaxations in glass state at  $T < T_g$ , which is also utilized to understand the GGI structures in micro- and nano-structured Co–Fe–Ni–P samples.

According to the characteristics of structural relaxation in BMG, it can be seen that an increase of index  $n$  attributed to solid-like glassy grain interiors has not been observed around  $T_g$  in samples #3 to #4 with a larger  $D_{avg}$ , indicating the decreasing trend observed at this range is mainly contributed by GGIs that generally promote glass transition. However, samples #1 to #2 with a smaller  $D_{avg}$  are identified to exhibit similar features of structural relaxation as BMG at  $T < T_g$ , which could be caused by the altered glass state in their GGI regions and may be explained by the relations between  $\eta$  and index  $n$ , as shown in Figures 11(b) through (e). Specifically, for samples #1–#2 with a reduced  $D_{avg}$ , their  $\eta$  values are found to increase with decreasing index  $n$  at  $T < T_g$ , suggesting that the free volumes at GGI regions are much reduced in the formation of nano-structures so that atomic structures of GGIs are dominated by solid-like clusters similar with those in BMG and at the interior of glassy grains. On the contrary, for samples #3 to #4 with a greater  $D_{avg}$ , as shown in Figures 11(d) and (e), their  $\eta$  would increase with increasing index  $n$  at  $T < T_g$ , suggesting that most free volumes at GGI regions are maintained in the formation of heterogenous structures so that atomic structures of GGIs are dominated by liquid-like clusters similar with those in their SC-liquid state ( $T_g < T < T_x$ ). The atomic structures at GGIs in both micro- and nano-structured samples are well reflected by Eq. [2] through [4]. Since GGIs in samples #1 to #2 behave in a similar manner as thermodynamically stable BMG, the obtained results, thus, illustrate the fact that nano-sized glassy grains are interconnected by GGIs with a thermodynamically stable glass phase. On the contrary, glassy grains in samples #3 to #4 might be loosely bonded by GGIs with a thermodynamically unstable glass phase. Furthermore, it is found that the GGI structures in sample #2 differ from those in sample #3, suggesting that a critical size  $D_c$  for  $D_{avg}$  of glassy grains must exist<sup>[65]</sup> and could be characterized to be  $D_c \sim 200$  nm for amorphous Co–Fe–Ni–P alloys, below which the solid-like GGI structures could be formed in the nano-structured samples. To be specific, when two adjacent grains are bonding, atoms at shell

regions of glassy grains with  $D_{avg} > D_c$  are less mobile and, as a result, interfacial atoms formed between these glassy grains are far from their equilibrium positions, thereby increasing the free volumes and reducing the thermodynamic stability of atomic clusters at liquid-like GGIs. On the contrary, resulted from the fast surface dynamics in glassy grains  $D_{avg} < D_c$ , GGIs formed are more likely to be thermodynamically stable and relatively dense, manifesting themselves with dominant solid-like atomic clusters as compared to GGIs in samples containing larger glassy grains. Due to the high diffusivity of surface atoms before transforming into GGIs of NGs ( $D_{avg} < 100$  nm), although these interfacial regions still have excess free volumes, GGI areas may be in a glass state which is more thermodynamically stable than those of grain interiors or BMGs. Therefore, GGIs may be enriched with free volumes while their atomic structures in the glass state are dominated with solid-like atomic clusters (and with much less liquid-like atomic clusters).

### C. Size-Effects on GFA as Characterized by Structural Relaxations in the SC-Liquid State

The effects of  $D_{avg}$  on structural relaxation of NGs in SC-liquid state may also be analyzed to reveal the GFAs of NGs. At  $T_g < T < T_x$ ,  $\eta$  decreases with decreasing index  $n$ , suggesting that there are vanishing solid-like clusters when  $T_x$  is approached. Particularly, sample #1 at a temperature approaching  $T_x$  is more liquid like compared to samples #2 to #4, manifesting itself with a relatively small  $\eta$  at  $T_x$ , for example,  $\eta = 1.9$  GPa·s compared to that (5.2 GPa·s) of micro-structured sample #4. It is argued that a lower  $\eta$  of the SC-liquid at  $T_x$  has a weaker tendency for it to transform into a crystalline phase and, thus, a larger  $\Delta T = T_x - T_g$  or better stability of NGs, which agrees with the previous finding from DSC as listed in Table I.

The GFAs of Co–Fe–Ni–P NGs are described by another parameter called index  $\beta$ , as determined by the dynamical scaling for  $Q^{-1}$  of NGs in SC-liquid state, which is proposed in our previous work,<sup>[65]</sup> as follows:

$$Q^{-1}(T_x) = A(\dot{T})(\dot{T}/\omega)^\beta, \quad [7]$$

where  $\dot{T}$  is the heating rate and  $A(\dot{T})$  is the transition temperature dependence on  $\dot{T}$  such as  $T_x$ . It is worth noting that the feasibility and sensitivity of this parameter have been verified by conventional MGs and those with  $\beta > 0.4$  are found to be good glass formers that can be made into BMGs.<sup>[65]</sup> As it is seen from Figure 12(a), the results show a good linearity of fitting for Co–Fe–Ni–P NGs using Eq. [7]. Their corresponding index  $\beta$  is illustrated in Figure 12(b), which are 0.265, 0.186, 0.171, and 0.151 for samples #1 to #4, respectively. In general, a higher index  $\beta$  indicates a better GFA of the glassy alloys. Since the GGIs are more thermodynamically stable in NGs with reduced  $D_{avg}$ , nano-structured Co–Fe–Ni–P samples would be expected to have a better GFA, thus, a higher index  $\beta$ . Furthermore, based on the relation between index  $\beta$  and  $D_{avg}$ , which is a fitted curve shown in Figure 12(b), NGs with  $D_{avg} < 40$  nm could become a good glass former compatible to BMGs with  $\beta > 0.4$ .<sup>[65]</sup>



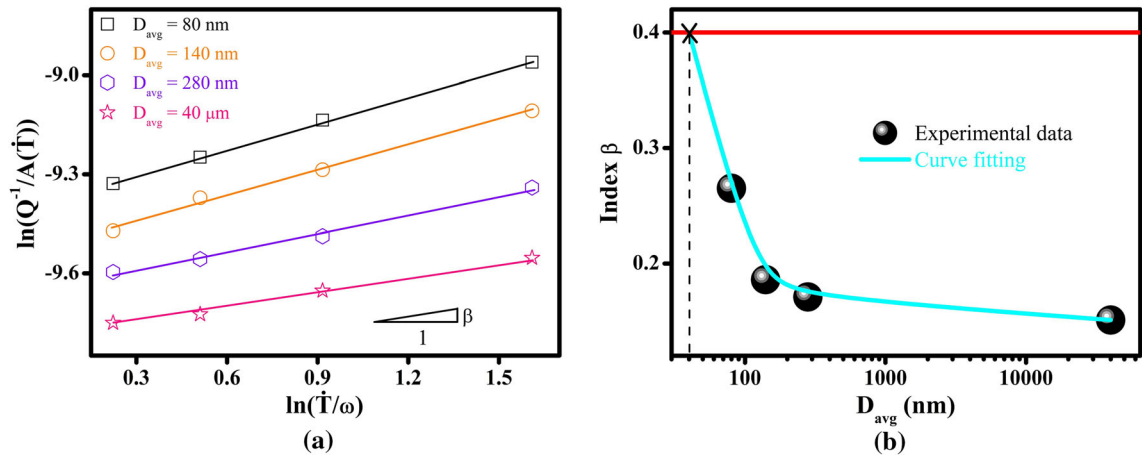


Fig. 12—(a) Dynamic scaling for  $Q^{-1}(T_x)$  and (b) index  $\beta$  for samples #1 to #4 with different  $D_{avg}$ . The red line marks the critical (least) index  $\beta$  for BMGs.<sup>[65]</sup>  $D_{avg} = 40$  nm at the cross point (Color figure online).

Thus, it is possible to prepare NGs in a bulk form by pulse electrodeposition or powder metallurgy techniques through reducing the sizes of glassy grains or nanoparticles to below 40 nm.

#### IV. CONCLUSION

Anelastic behaviors related with the structural relaxation of GGIs in Co–Fe–Ni–P NGs are systematically investigated by mechanical spectrum, which have been successfully synthesized by a pulse electrodeposition method. The results provide direct evidences that a new glass phase could be formed at GGIs in NGs, as characterized by an activation energy (0.91 eV) for glass transition at GGIs much different with that (1.99 eV) in the interiors of glassy grains. It is found that the atomic structures at GGIs in NGs with  $D_{avg} < 150$  nm are much different with those in NGs with  $D_{avg} > 250$  nm, suggesting that a critical size of  $D_{avg}$ , *i.e.*,  $D_c \sim 200$  nm, may exist. Analyses on atomic structures suggest that GGIs would transform from a thermodynamically unstable glass phase in NGs with  $D_{avg} > D_c$  to a thermodynamically stable glass phase in NGs with  $D_{avg} < D_c$ . As a result, GFAs of NGs improve with decreasing  $D_{avg}$ , which can be quantitatively measured by the dynamical scaling for mechanical losses in the SC-liquid state, and it is predicted that Co–Fe–Ni–P NGs with  $D_{avg} < 40$  nm are good glass formers, compatible to BMGs. The results, thus, give a better understanding on the atomic structures of NGs particularly at GGIs, which is helpful to resolve the strength and ductility trade-off dilemma in NGs.

#### ACKNOWLEDGMENTS

This work was supported by a grant from the Research Grants Council of the Hong Kong Special Administrative Region, China (PolyU152607/16E).

#### DATA AVAILABILITY

The datasets generated and/or analyzed during the current study are available from the corresponding author on reasonable request.

#### CONFLICT OF INTEREST

The authors have no conflicts of interest to declare that are relevant to the content of this article.

#### REFERENCES

1. H. Gleiter: *Beilstein J. Nanotechnol.*, 2013, vol. 4, pp. 517–33.
2. H. Gleiter, T. Schimmel, and H. Hahn: *Nano Today*, 2014, vol. 9, pp. 17–68.
3. N. Chen, D.V. Louzguine-Luzgin, and K. Yao: *J. Alloys Compd.*, 2017, vol. 707, pp. 371–78.
4. T. Feng, H. Hahn, and H. Gleiter: *Acta Phys. Sin.*, 2017, vol. 66, p. 176110.
5. S.V. Ketov, X. Shi, G. Xie, R. Kumashiro, A.Y. Churyumov, A.I. Bazlov, N. Chen, Y. Ishikawa, N. Asao, H. Wu, and D.V. Louzguine-Luzgin: *Sci. Rep.*, 2015, vol. 5, p. 7799.
6. K. Wu, F. Chu, Y. Meng, K. Edalati, Q. Gao, W. Li, and H.-J. Lin: *J. Mater. Chem. A*, 2021, vol. 9, pp. 12152–60.
7. X. Wang, F. Jiang, H. Hahn, J. Li, H. Gleiter, J. Sun, and J. Fang: *Scr. Mater.*, 2016, vol. 116, pp. 95–99.
8. Q. Hu, J. Wu, and B. Zhang: *Phys. B*, 2017, vol. 521, pp. 28–31.
9. F.C. Li, T.Y. Wang, Q.F. He, B.A. Sun, C.Y. Guo, T. Feng, and Y. Yang: *Scr. Mater.*, 2018, vol. 154, pp. 186–91.
10. C. Guo, Y. Fang, F. Chen, and T. Feng: *Intermetallics*, 2019, vol. 110, p. 106480.
11. C. Pei, R. Zhao, Y. Fang, S. Wu, Z. Cui, B. Sun, S. Lan, P. Luo, W. Wang, and T. Feng: *J. Alloys Compd.*, 2020, vol. 836, p. 155506.
12. S.P. Singh, M.R. Chellali, L. Velasco, Y. Ivanisenko, E. Boltynjuk, H. Gleiter, and H. Hahn: *J. Alloys Compd.*, 2020, vol. 821, p. 153486.
13. T. Li and G. Zheng: *Metall. Mater. Trans. A*, 2021, vol. 52, pp. 1939–46.
14. Q. Yang, C.-Q. Pei, H.-B. Yu, and T. Feng: *Nano Lett.*, 2021, vol. 21, pp. 6051–56.
15. S.H. Nandam, R. Schwaiger, A. Kobler, C. Kübel, C. Wang, Y. Ivanisenko, and H. Hahn: *J. Mater. Res.*, 2021, vol. 36, pp. 2903–14.
16. J.L. Ma, H.Y. Song, M.R. An, W.W. Li, and R.Q. Han: *J. Non. Cryst. Solids*, 2021, vol. 553, p. 120464.

17. S. Yuan and P.S. Branicio: *Scr. Mater.*, 2021, vol. 194, p. 113639.
18. O. Adjaoud and K. Albe: *Front. Mater.*, 2021, vol. 8, p. 664220.
19. C. Kalcher, O. Adjaoud, and K. Albe: *Front. Mater.*, 2020, vol. 7, p. 223.
20. S. Yuan and P.S. Branicio: *Int. J. Plast.*, 2020, p. 102845.
21. S.D. Feng, Y.D. Liu, L.M. Wang, and R.P. Liu: *J. Non. Cryst. Solids*, 2020, vol. 546, p. 120265.
22. A. Baksi, S.H. Nandam, D. Wang, R. Kruk, M.R. Chellali, J. Ivanisenko, I. Gallino, H. Hahn, and S. Bag: *ACS Appl. Nano Mater.*, 2020, vol. 3, pp. 7252–59.
23. M. Ghafari, X. Mu, J. Bednarcik, W.D. Hutchison, H. Gleiter, and S.J. Campbell: *J. Magn. Magn. Mater.*, 2020, vol. 494, p. 165819.
24. J. Cheng, T. Li, S. Ullah, F. Luo, H. Wang, M. Yan, and G. Zheng: *Nanotechnology*, 2020, vol. 31, p. 385704.
25. J.Q. Wang, N. Chen, P. Liu, Z. Wang, D.V. Louzguine-Luzgin, M.W. Chen, and J.H. Perepezko: *Acta Mater.*, 2014, vol. 79, pp. 30–36.
26. M. Mohri, D. Wang, J. Ivanisenko, H. Gleiter, and H. Hahn: *J. Alloys Compd.*, 2018, vol. 735, pp. 2197–2204.
27. S.H. Nandam, O. Adjaoud, R. Schwaiger, Y. Ivanisenko, M.R. Chellali, D. Wang, K. Albe, and H. Hahn: *Acta Mater.*, 2020, vol. 193, pp. 252–60.
28. M. Mohri, M.R. Chellali, D. Wang, and J. Ivanisenko: *Met. Mater. Int.*, 2021.
29. T. Li, K. Ma, and G. Zheng: *J. Mater. Res.*, 2021, vol. 36, pp. 4951–62.
30. H. Gleiter: *Small*, 2016, vol. 12, pp. 2225–33.
31. N. Chen, D. Wang, T. Feng, R. Kruk, K.F. Yao, D.V. Louzguine-Luzgin, H. Hahn, and H. Gleiter: *Nanoscale*, 2015, vol. 7, pp. 6607–11.
32. S.H. Nandam, Y. Ivanisenko, R. Schwaiger, Z. Śniadecki, X. Mu, D. Wang, R. Chellali, T. Boll, A. Kilmametov, T. Bergfeldt, H. Gleiter, and H. Hahn: *Acta Mater.*, 2017, vol. 136, pp. 181–89.
33. Z. Śniadecki, D. Wang, Y. Ivanisenko, V.S.K. Chakravadhanula, C. Kübel, H. Hahn, and H. Gleiter: *Mater. Charact.*, 2016, vol. 113, pp. 26–33.
34. M. Mohri, D. Wang, J. Ivanisenko, H. Gleiter, and H. Hahn: *Mater. Charact.*, 2017, vol. 131, pp. 140–47.
35. X.D. Wang, Q.P. Cao, J.Z. Jiang, H. Franz, J. Schroers, R.Z. Valiev, Y. Ivanisenko, H. Gleiter, and H.J. Fecht: *Scr. Mater.*, 2011, vol. 64, pp. 81–84.
36. H. Shao, Y. Xu, B. Shi, C. Yu, H. Hahn, H. Gleiter, and J. Li: *J. Alloys Compd.*, 2013, vol. 548, pp. 77–81.
37. C. Guo, Y. Fang, B. Wu, S. Lan, G. Peng, X.L. Wang, H. Hahn, H. Gleiter, and T. Feng: *Mater. Res. Lett.*, 2017, vol. 5, pp. 293–99.
38. O. Franke, D. Leisen, H. Gleiter, and H. Hahn: *J. Mater. Res.*, 2014, vol. 29, pp. 1210–16.
39. A. Sharma, S.H. Nandam, H. Hahn, and K.E. Prasad: *Scr. Mater.*, 2021, vol. 191, pp. 17–22.
40. X.L. Wang, F. Jiang, H. Hahn, J. Li, H. Gleiter, J. Sun, and J.X. Fang: *Scr. Mater.*, 2015, vol. 98, pp. 40–43.
41. K. Albe, Y. Ritter, and D. Şopu: *Mech. Mater.*, 2013, vol. 67, pp. 94–103.
42. S. Adibi, P.S. Branicio, Y.W. Zhang, and S.P. Joshi: *J. Appl. Phys.*, 2014, vol. 116, p. 043522.
43. S. Adibi, P.S. Branicio, and S.P. Joshi: *Sci. Rep.*, 2015, vol. 5, p. 15611.
44. K. Zheng and P. Branicio: *Phys. Rev. Mater.*, 2020, vol. 4, p. 076001.
45. C. Wang, D. Wang, X. Mu, S. Goel, T. Feng, Y. Ivanisenko, H. Hahn, and H. Gleiter: *Mater. Lett.*, 2016, vol. 181, pp. 248–52.
46. X. Mu, L. Chen, R. Mikut, H. Hahn, and C. Kübel: *Acta Mater.*, 2021, vol. 212, p. 116932.
47. J.X. Fang, U. Vainio, W. Puff, R. Würschum, X.L. Wang, D. Wang, M. Ghafari, F. Jiang, J. Sun, H. Hahn, and H. Gleiter: *Nano Lett.*, 2012, vol. 12, pp. 458–63.
48. Y. Ritter, D. Opu, H. Gleiter, and K. Albe: *Acta Mater.*, 2011, vol. 59, pp. 6588–93.
49. K. Zheng, S. Yuan, H. Hahn, and P.S. Branicio: *Sci. Rep.*, 2021, vol. 11, p. 19246.
50. R. Witte, T. Feng, J.X. Fang, A. Fischer, M. Ghafari, R. Kruk, R.A. Brand, D. Wang, H. Hahn, and H. Gleiter: *Appl. Phys. Lett.*, 2013, vol. 103, p. 073106.
51. C. Liu, E. Pineda, and D. Crespo: *Metals*, 2015, vol. 5, pp. 1073–1111.
52. E. Bonetti: *Philos. Mag. B*, 1987, vol. 56, p. 185.
53. H. Okumura, H.S. Chen, A. Inoue, and T. Masumoto: *Jpn. J. Appl. Phys.*, 1991, vol. 30, pp. 2553–57.
54. Y. He and X. Li: *Phys. Status Solidi*, 1987, vol. 99, pp. 115–20.
55. X.-G. Li, Y. Zhang, and Y. He: *J. Phys. Condens. Matter*, 1990, vol. 2, pp. 809–16.
56. Q. Wang, S.T. Zhang, Y. Yang, Y.D. Dong, C.T. Liu, and J. Lu: *Nat. Commun.*, 2015, vol. 6, p. 7876.
57. Y. Ueno, M. Hojo, H. Numakura, T. Ichitsubo, and J. Saida: *Mater. Sci. Eng. A*, 2009, vol. 521–522, pp. 232–35.
58. B. Cai, L.Y. Shang, P. Cui, and J. Eckert: *Phys. Rev. B*, 2004, vol. 70, p. 184208.
59. Q. Wang, J.M. Pelletier, Y. Da Dong, Y.F. Ji, and H. Xiu: *Mater. Sci. Eng. A*, 2004, vol. 379, pp. 197–203.
60. Z. Wang, D. Wang, P. Jiang, W. Wu, X. Li, F. Zu, and J. Shui: *J. Wuhan Univ. Technol. Sci. Ed.*, 2017, vol. 32, pp. 1476–80.
61. M.A. Meyers and K.K. Chawla: *Mechanical Behavior of Materials*, 1999.
62. C.W. Macosko: *Rheology: Principles, Measurements, and Applications*, 1996.
63. A. Nowick and B.S. Berry: *Anelastic Relaxation in Crystalline Solids*, 1972.
64. N. Chen, D. Wang, P.F. Guan, H.Y. Bai, W.H. Wang, Z.J. Zhang, H. Hahn, and H. Gleiter: *Appl. Phys. Lett.*, 2019, vol. 114, p. 043103.
65. T. Li, Y. Shen, and G. Zheng: *Scr. Mater.*, 2021, vol. 203, p. 114109.

**Publisher's Note** Springer Nature remains neutral with regard to jurisdictional claims in published maps and institutional affiliations.